2 November 2001

Chemical Physics Letters 348 (2001) 27–33

CHEMICAL PHYSICS LETTERS

www.elsevier.com/locate/cplett

Polydisperse Au nanoclusters on silicon: fractal aggregates via spinodal decomposition?

M.D.R. Taylor [a], P. Moriarty [a,*], M. Brust [b]

[a] *School of Physics and Astronomy, University of Nottingham, Nottingham NG7 2RD, UK*
[b] *Department of Chemistry, University of Liverpool, Crown Street, Liverpool L69 7ZD, UK*

Received 2 July 2001; in final form 9 July 2001

Abstract

Deposition of polydisperse Au nanoclusters onto Si via condensation from toluene produces aggregates that may be structurally characterised in terms of their fractal dimension (D_f). Atomic force microscopy reveals a transition (as a function of position on the sample surface) from a percolating, gel-like cluster network to isolated, low D_f aggregates, highlighting the key role that *local* cluster concentration plays in determining the morphology of nanocluster arrays. Although the fractal dimension values measured are consistent with nucleation processes, the cluster layer morphologies bear a striking resemblance to the patterns observed following spinodal decomposition of polymer blends and binary fluid mixtures.

1. Introduction

Ordered macroscopic arrays of passivated or functionalised colloidal nanoclusters are currently vaunted as the basis of novel 'designer materials' whose physical properties may be tuned by controlling the size, spacing and ordering of their constituent clusters [1]. A fundamental motivation underlying the recent rapid progress in the synthesis of well ordered nanocluster arrays is the development of a viable nanoscale electronics technology. Hence, the electrical transport characteristics – specifically, the Coulomb blockade and Coulomb staircase behaviour – of thiol-derivatised Au nanoclusters [2] adsorbed on a range of substrates [3–5] have been extensively studied.

Of primary importance to the development of cluster-based nanostructured materials and nanoelectronic device architectures is the arrangement of the nanoparticles on a substrate. Thus, the dependence of the self-assembly of surfactant-stabilised nanoclusters on mean cluster size, cluster size distribution, cluster concentration and solvent type has been studied in some depth [6–9] for size-selected nanoparticles. Two studies of crystal formation from solutions of *polydisperse* Au nanoparticles are of particular relevance to the work reported in this Letter. Ohara et al. [10] observed that the size dependence of the intercluster interactions for dodecanethiol-passivated gold nanoparticles was sufficient to promote

* Corresponding author. Fax: +44-115-9515180.
E-mail address: philip.moriarty@nottingham.ac.uk (P. Moriarty).

0009-2614/01/$ - see front matter
PII: S0009-2614(01)01055-7

size-selective crystallisation and phase separation, producing small radially ordered opals. More recently, Kiely et al. [11] demonstrated that polydisperse Au nanocrystals similarly passivated with dodecanethiol could, remarkably, spontaneously crystallise into long range-, *bimodally* ordered structures on amorphous carbon substrates.

Here we report that for *identically prepared* cluster solutions as those used by Kiely et al., following drop deposition onto Si surfaces, we observe neither radial nor bimodal ordering of the Au nanocrystals. Instead, the Au particles form aggregates whose fractal dimension shows a large variation across the surface. While the observation of aggregates with fractional dimension in our study might at first be thought of as indicative of diffusion- or reaction-limited aggregation [12,13], the morphologies of the Au nanocluster overlayers are highly reminiscent of those observed in studies of spinodal decomposition of polymer blends [14] and binary fluid mixtures [15]. Furthermore, Ge and Brus [16] have recently explained the formation of CdSe nanoparticle films in terms of spinodal decomposition processes.

Spinodal decomposition is the means by which phase separation takes place in a binary fluid mixture or a homogeneous fluid when it is quenched into an unstable region of its phase diagram [17]. A closely related phenomenon is spinodal dewetting where a thin film breaks up due to thermal fluctuations at its surface, producing height variations analogous to the composition fluctuations observed in spinodal decomposition in fluid mixtures [18]. While it is important to distinguish both spinodal decomposition and spinodal dewetting from nucleation processes, due to the similarities between the structures produced via aggregation/gellation and spinodal decomposition, this can be rather problematic. We return to this point below.

2. Experimental

Polydisperse solutions of dodecanethiol-passivated Au nanocrystals, prepared as described in [2] were used throughout. A 20 μl drop of the nanocrystal solution (concentration $\sim 10^{17}$ clusters/l) was deposited onto either an untreated Si(1 1 1) substrate, covered with a native oxide layer, or a hydrogen-passivated Si(1 1 1) surface – in each case the samples were 0.7 cm^2 in area. Although, as described below, uniform coverage of the sample does not occur in our experiments, the amount of material deposited is equivalent to ~ 1 complete close packed layer of nanocrystals on the sample surface. No steps were taken to slow the natural evaporation rate of the solvent [9]. The H:Si(1 1 1) surface was prepared using well-established methods [19].

Non-contact/tapping mode atomic force microscope (AFM) (NC-AFM) studies of the adsorbed nanocrystals were carried out using Topometrix and Digital Instruments systems [20]. Typical scan speeds were 2–10 μm s^{-1}. Scanning tunnelling microscope (STM) measurements were carried out using a home-built STM under high vacuum conditions (10^{-8} Torr). Although images of submonolayers of clusters on H:Si(1 1 1) in air could be acquired, these were substantially more noisy and irreproducible compared to STM data acquired under vacuum.

3. Results and discussion

STM imaging of submonolayer coverages of nanoclusters on H:Si(1 1 1) (produced by a 1:20 dilution of the original cluster solution in toluene) was used to ascertain the size distribution of the polydisperse particles employed in our study (see Fig. 1). We take the cluster height in the STM image as a measure of nanoparticle diameter as this alleviates uncertainties due to tip-particle convolution effects. It is clear from the histogram shown in Fig. 1 that the particles have a broad size distribution – a Gaussian fit to the data produces a mean particle diameter of 6.1($\pm$0.2) nm and a standard deviation of 30($\pm$8)%. Fig. 1d is an STM image of a different region of the sample from which Fig. 1a was acquired. Both 2D and 3D aggregates are observed, clearly illustrating that *local* cluster concentration plays an important role in the morphology of nanocluster overlayers on surfaces. This is quite different from Taleb et al. [5] recent report of control of the dimensionality of

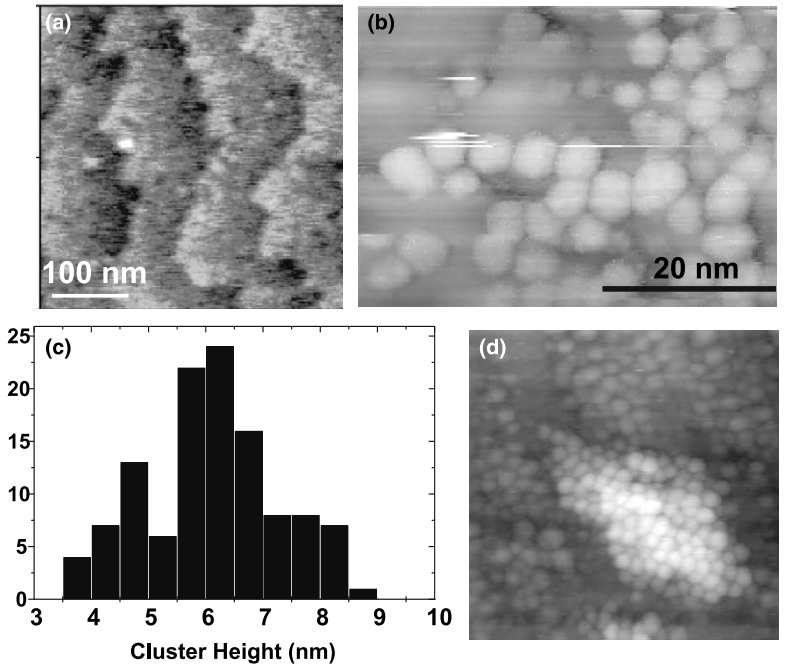

Fig. 1. (a) Non-contact AFM image of the H:Si(1 1 1) surface prior to deposition of clusters. Single-height atomic steps separating terraces ~100 nm in width are visible. (b) STM image of a submonolayer coverage of passivated Au nanocrystals on H:Si(1 1 1). A number of similar images were used to generate the histogram of cluster heights shown in (c). (d) STM image ($V = -3$ V, $I = 0.1$ nA) of the coexistence of 2D (lower left and upper right of image) and 3D (bottom half of image) nanocluster aggregates on H:Si(1 1 1). Note the absence of radial or bimodal ordering in the aggregates.

nanoparticle aggregates effected via changes in the concentration of particles in solution *prior to deposition*. Local cluster concentration will be determined by the interplay of spreading coefficient, dewetting, and nanoparticle diffusion (convective currents seemingly do not play a role [8]) and thus control of the dimensionality of Au nanocluster overlayers requires consideration of a wider range of factors than just the particle concentration in solution. Note also from Fig. 1d that there is no evidence for radial [10] or bimodal [11] ordering of polydisperse Au nanocrystals on H:Si(1 1 1).

Fig. 2 shows four representative 2×2 μm^2 images of a nanocluster overlayer on SiO_2 produced by deposition of a drop of the undiluted cluster solution on the substrate. Following acquisition of the image shown in Fig. 2a, the tip was retracted, the sample moved laterally by approximately 100 μm, the tip then restored to feedback and the image shown in Fig. 2b was acquired. This process was repeated for Fig. 2c,d. To eliminate the possibility

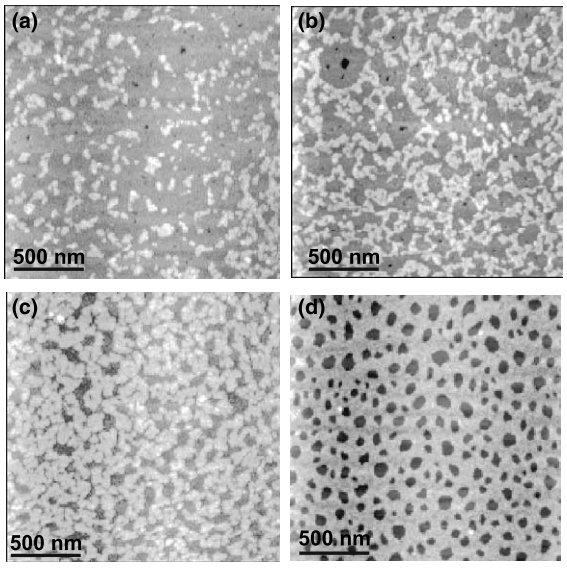

Fig. 2. Non-contact mode AFM (NC-AFM) images (each 2×2 μm^2) illustrating the variation in surface morphology following deposition of polydisperse Au nanocrystals on SiO_2.

that modifications of the tip structure induced by repeated scanning played a role in the morphological changes we observed, following acquisition of Fig. 2d the tip was returned to the vicinity of the area scanned in Fig. 2a and another image was taken. The morphological variations shown in Fig. 2 were entirely reproducible following repeated scanning with the same tip. In addition, a number of different tips were used and each reproduced the general features of the images shown in Fig. 2.

An important point – and one that may not be immediately apparent from the images shown in Fig. 2 – is that the cluster films formed from deposition of the undiluted cluster solution on SiO_2 are >1 monolayer thick. A number of holes are observed in the 'substrate' in Fig. 2a,b – a particularly prominent example is seen in the top left hand corner of Fig. 2b. These holes, as measured from AFM line profiles, are $6(\pm 1)$ nm deep.

It is clear from the images shown in Fig. 2a–c that nanocluster aggregation has not resulted in the formation of close-packed, long-range-ordered islands or 'rafts' as observed for polydisperse nanoclusters deposited on amorphous carbon substrates [11]. Rather, the aggregates have a distinct ramified appearance (see, in particular, Figs. 2b and 4) and are best described as fractal objects. The fractal character of 3D colloidal aggregates has been investigated in recent years using a number of techniques [13,21,22]. There are two aspects of that work that should be noted with regard to the present study. First, a variety of aggregation models have been elucidated – the diffusion-limited aggregation (DLA) model first proposed by Witten and Sander [12] has been augmented by a number of kinetically limited aggregation modes (including reaction limited cluster aggregation (RLCA)) each producing a signifi-

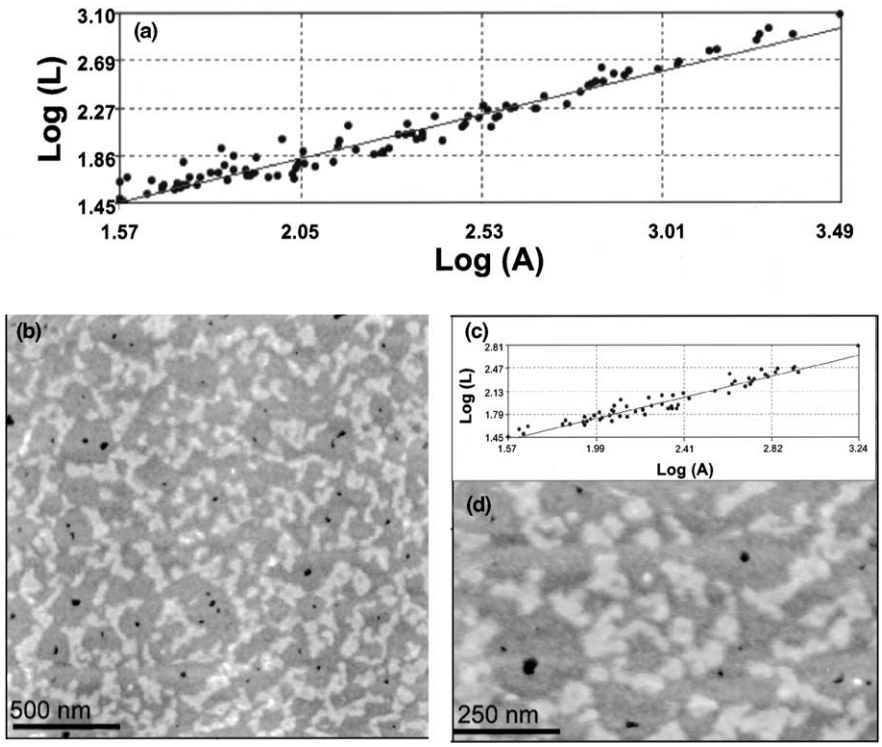

Fig. 3. (a) A plot of log (perimeter length) vs log (area) for the aggregates shown in (b), a 2×2 μm^2, 500×500 pixel NC-AFM scan, yields $D_f = 1.5 \pm 0.1$. The plot shown in (c) yields a value of $D_f = 1.52 \pm 0.08$ and was derived from a smaller, lower resolution scan (1 μm^2, 300×300 pixels), part of which is shown in (d).

cantly different aggregate morphology [13]. A second important feature of recent work on 3D fractal aggregation in colloidal systems has been the investigation of the role of the volume fraction. Both van Garderen et al. [22] and Kolb and Hermann [23] have demonstrated that increasing the volume fraction leads to an increase in the value of D_f.

We have used the perimeter–area method to determine the fractal dimension of the 2D Au nanocluster aggregates that form on Si surfaces. Briefly, the relationship between the perimeter length L, and area A, of a fractal aggregate is given by

$$L(\delta) = \alpha D_f A^{D_f'/2},$$

where D_f is the fractal dimension of the aggregate, α is a constant and δ is the yardstick length (in the case of the images used in our study, δ corresponds to the pixel length in nm). A plot of log L vs log A then yields the fractal dimension. The restriction on δ employed by Gomez-Rodriguez et al. [24], namely, that aggregates with $A < 30\delta^2$ are discarded from the analysis, was used to ensure that the finite radius of curvature of the tip did not affect the measurement of the fractal dimension [25].

Figs. 3a and b are a 2×2 μm^2, 500×500 pixel scan and a corresponding log L vs log A plot, respectively. The latter yields a fractal dimension of 1.5 ± 0.1 for the aggregates. A smaller area (1 μm^2) scan (300×300 pixels) and log L vs log A plot of the same surface region similarly yields a fractal dimension of 1.52 ± 0.08 (Figs. 3c and d). However, calculation of D_f for the image shown in Fig. 2c yields a value of 1.8 ± 0.1. This increase in the value of D_f is consistent with the significantly more compact aggregates shown in Fig. 2c as compared to those shown in either Fig. 2b or Fig. 3. From a DLA/RLCA perspective, the increase in D_f we observe, in analogy with light scattering and numerical studies of 3D colloidal aggregation [21–23], arises from a local increase in volume fraction i.e., cluster concentration. One possible origin of the 2D morphology in Fig. 2c is the coalescence of isolated fractal aggregates forming a space-spanning porous macrocluster or 'gel-like' state. Of particular interest in terms of the fundamental electrical transport properties of the Au cluster overlayers is that Fig. 2c represents a system at or very near its percolation threshold. Note that spin coating of a more dilute concentration of clusters (10^{16}/l) produces *submonolayer* nanocluster coverages. These samples again exhibit fractal aggregates, but with a significantly lower value of fractal dimension (Fig. 4, $D_f = 1.3 \pm 0.1$). Furthermore, very little variation in the fractal dimension value was observed across the sample surface.

Thus far we have described the nanocrystal aggregates we observe in terms of DLA and its variants. However, an alternative explanation is that the spatial distribution of the Au clusters arises from spinodal decomposition. In that case, instead of Fig. 2a–c representing early-, mid- and late stages of a DLA (or reaction limited aggregation) process, respectively, the cluster distributions correspond to various stages of spinodal decomposition. Fig. 2c in particular bears a striking resemblance to the highly inter-connected patterns observed in the early stages of phase separation of binary fluids [15]. Coarsening then leads to the inter-connected regions breaking up

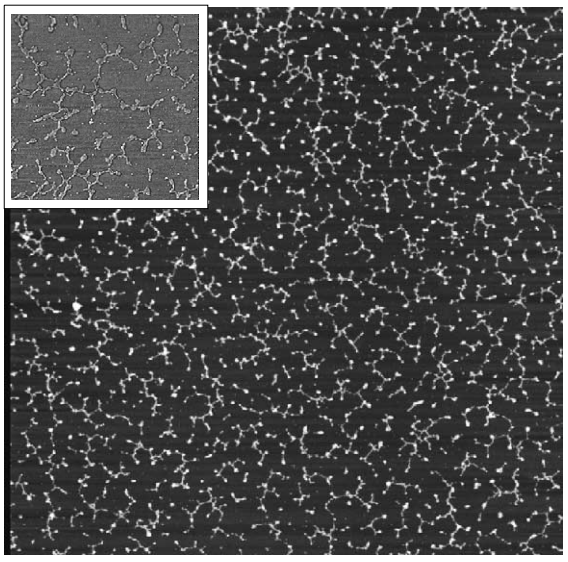

Fig. 4. 8.7×8.7 μm^2 tapping mode image of Au nanocluster aggregates produced via spin coating of ~10 μl of a 10^{16}/l concentration solution onto a native oxide covered Si(1 1 1) sample. Inset: 2×2 μm^2 phase image.

and producing structures similar to those shown in Figs. 2a,b and 3. However, regardless of the mechanism of nanocluster aggregate production, variations in local cluster concentration remain the most plausible explanation for the changes in morphology across the sample surface shown in Fig. 2.

Without a detailed study of the kinetics of the dewetting process including, in particular, an analysis of the temporal variation of the in-plane correlation length associated with the cluster aggregates, it is difficult to unambiguously identify whether diffusion-limited aggregation, nucleation or spinodal decomposition or a combination is responsible for the structures observed in Figs. 2 and 3. However, we note that across limited ranges of cluster concentrations it is possible to quench the system directly into a metastable state where phase transitions are nucleation driven (see Fig. 1 of [17] or Fig. 4 of [16]). This might then explain the 'polygonal' network of holes observed in Fig. 2d – a common result of nucleation driven dewetting [26]. On a related point, close examination of Figs. 2a,b, and 3b,d reveals that each $\sim$6 nm deep hole in the continuous nanocluster layer that supports the aggregates is surrounded by a 'denuded' zone, i.e., a region free of clusters. This is also suggestive of nucleated dewetting with the holes acting as nucleation centres. We are currently carrying out experiments with a range of solvents and cluster concentrations in order to elucidate the relative importance of dewetting, nucleation and spinodal decomposition in the formation of nanocrystal aggregates and overlayers.

4. Conclusion

Scanning probe measurements of polydisperse Au nanocrystals deposited on Si surfaces reveal the formation of aggregates that may be characterised in terms of their fractal dimension. Differences in the fractal dimension of the aggregates across the surface are attributed to variations in the local cluster concentration. Although the morphologies of the cluster overlayers are highly suggestive of aggregate formation via spinodal decomposition, further structural studies are required to identify the degree to which nucleation, dewetting and DLA/RLCA processes contribute. Our results highlight both the complexity of the aggregation processes at the solid–liquid interface and the large parameter space that must be considered if nanocluster overlayers with a specific, pre-determined morphology are to be controllably synthesised on silicon.

Acknowledgements

This work was funded by the UK Engineering and Physical Sciences Research Council (EPSRC). We thank Peter Beton for a critical reading of an early version of the manuscript and for helpful discussion.

References

[1] A.P. Alivisatos, Science 271 (1996) 933.
[2] M. Brust, M. Walker, D. Bethell, D.J. Schiffrin, R. Whyman, J. Chem. Soc., Chem. Commun. (1994) 801; M. Brust, D. Bethell, D.J. Schiffrin, C. Kiely, Adv. Mater. 7 (1995) 795.
[3] P.J. Durston, J. Schmidt, R.E. Palmer, J.P. Wilcoxon, Appl. Phys. Lett. 71 (1997) 2940.
[4] L.E. Harrell, T.P. Bigioni, W.G. Cullen, R.L. Whetten, P.N. First, J. Vac. Sci. Tech. B 17 (1999) 2411.
[5] A. Taleb, F. Silly, A. Gusev, F. Charra, M. Pileni, Adv. Mater. 12 (2000) 633.
[6] R.P. Andres, T. Bein, M. Dorogi, S. Feng, J.I. Henderson, C.P. Kubiak, W. Mahoney, R.G. Osifchin, R. Reifenberger, Science 272 (1996) 1323.
[7] C.B. Murray, C.R. Kagan, M.G. Bawendi, Science 270 (1995) 1335.
[8] B.A. Korgel, D. Fitzmaurice, Phys. Rev. Lett. 80 (1998) 3531.
[9] X.M. Lin, H.M. Jaeger, C.M. Sorensen, K.J. Klabunde, J. Phys. Chem. B 105 (2001) 3353.
[10] P.C. Ohara, D.V. Leff, J.R. Heath, W.M. Gelbart, Phys. Rev. Lett. 75 (1995) 3466.
[11] C.J. Kiely, J. Fink, M. Brust, D. Bethell, D.J. Schiffrin, Nature 396 (1998) 444.
[12] T.A. Witten, L.M. Sander, Phys. Rev. Lett. 47 (1981) 1400.
[13] P. Meakin, J. Sol-Gel. Sci. Technol. 15 (1999) 97; J.C. Gimel, T. Nicolai, D. Durand, J. Sol-Gel. Sci. Technol. 15 (1999) 129.
[14] G. Krausch, C.-A. Dai, E.J. Kramer, F.S. Bates, Phys. Rev. Lett. 71 (1993) 3669, and references therein.

[15] A.J. Wagner, J.M. Yeomans, Phys. Rev. Lett. 80 (1998) 1429.
[16] G. Ge, L. Brus, J. Phys. Chem. B 104 (2000) 9573.
[17] S.W. Koch, R.C. Desai, F.F. Abraham, Phys. Rev. A 27 (1983) 2152; S. Puri, K. Binder, Phys. Rev. E 49 (1994) 5359.
[18] R. Xie, A. Karim, J.F. Douglas, C.C. Han, R.A. Weiss, Phys. Rev. Lett. 81 (1998) 1251.
[19] G.S. Higashi, Y.J. Chabal, G.W. Trucks, K. Raghavachari, Appl. Phys. Lett. 56 (1990) 656.
[20] A Topometrix Explorer (Figs. 2, 3) and a Digital Instruments MultiMode/ Nanoscope IIIa (Fig. 4) were used. Si cantilevers from MikroMasch (http://www.spmtips.com) with spring constants of $\sim$40 Nm^{-1} and resonant frequencies of 170–190 kHz were used.
[21] W.C.K. Poon, M.D. Haw, Adv. Colloid Interface Sci. 73 (1996) 71.
[22] H.F. van Garderen, W.H. Dokter, T.P.M. Beelen, R.A. Van Santen, E. Pantos, M.A.J. Michels, P.A.J. Hilbers, J. Chem. Phys. 102 (1995) 480.
[23] M. Kolb, J. Hermann, J. Phys. A 18 (1984) L435.
[24] J.M. Gomez-Rodriguez, A.M. Baro, L. Vazquez, R.C. Salvarezza, J.M. Vara, A.J. Arvia, J. Phys. Chem. 96 (1992) 347.
[25] In calculating the fractal dimension for a given region of the surface we have used a range of scan sizes and pixel densities to vary the value of δ. In each case we find that the calculated values of D_f agree within experimental error.
[26] U. Thiele, M. Mertig, W. Pompe, Phys. Rev. Lett. 80 (1998) 2869.